Journal of Solid State Chemistry **167,** 113–118 (2002)
doi:10.1006/jssc.2002.9629

Syntheses and Crystal Structures of $Er_2(SeO_3)_3$ and $Dy_3(SeO_3)_4F$

Ina Krügermann and Mathias S. Wickleder[1]

Institut für Anorganische Chemie, Universität zu Köln, Greinstrasse 6, D-50939 Köln, Germany

Received September 18, 2001; in revised form April 24, 2002; accepted May 2, 2002

The decomposition of $Er_2(SeO_4)_3$ in the presence of LiF in a sealed gold ampoule at 870°C yielded single crystals of $Er_2(SeO_3)_3$. The triclinic crystal structure ($P\bar{1}$, $Z = 2$, $a = 698.2(1)$, $b = 800.6(1)$, $c = 895.0(1)$ pm, $\alpha = 71.38(1)$, $\beta = 70.13(1)$, $\gamma = 65.87(1)^\circ$, $R_{all} = 0.0364$) contains two crystallographically different Er^{3+} ions in seven- and eightfold coordination of oxygen atoms, respectively. The distances Er–O range from 220 to 256 pm. Each of the three crystallographically different selenite groups connects four Er^{3+} ions with each other. The analogous reaction with $Dy_2(SeO_4)_3$ did not lead to the anhydrous selenite but to single crystals of the selenite fluoride $Dy_3(SeO_3)_4F$. In the hexagonal crystal structure ($P6_3mc$, $Z = 2$, $a = 1035.96(13)$, $c = 686.47(7)$ pm, $R_{all} = 0.0305$), one SeO_3^{2-} group and an F^- ion act as μ_3 ligands connecting three Dy^{3+} ions to triangles. The Dy^{3+} ions are coordinated by eight oxygen atoms and one fluoride ion with distances between 234 and 256 pm. The crystal structures are strongly influenced by the lone pairs of the SeO_3^{2-} ions. The IR spectra show the typical frequencies for selenite groups. © 2002 Elsevier Science (USA)

INTRODUCTION

Structural information of anhydrous rare earth compounds with complex anions are rare, especially for those compounds which are very temperature sensitive like perchlorates and chlorates. But also the far more stable sulfates of the rare earth elements are not very well characterized. As we have shown recently, the crystallization from a NaCl or LiF melt can be used to gain single crystals of anhydrous rare earth sulfates (1). This is, however, only true for the smaller lanthanides M= Dy−Lu, Y, Sc. Analogous reactions with the lighter lanthanides M= La, Ce–Tb always led to products containing additionally halide anions (2). Nevertheless, we have started to expand the crystallization from alkaline halide melts to other oxoanions, for example selenates. It turned out, that at reaction temperatures above 800°C not only the selenates crystallize from the melts but also the respective selenites, obviously due to the decomposition of the selenates (3). As has been shown for the example of lanthanum, from a sodium chloride melt one obtains $La_2(SeO_3)_3$ while single crystals of $LaFSeO_3$ form using lithium fluoride as a flux (4). The latter two compounds were the first anhydrous selenites which were structurally characterized, although compounds of the composition $M_2(SeO_3)_3$ have been mentioned previously. They had been prepared either by thermal decomposition of selenite hydrates (5), acidic selenites (6) or by fusing M_2O_3 and SeO_2 (6, 7). However, these methods did not lead to single crystals so that only powder diffraction data are available. Further investigations to extend the structural knowledge of the selenites throughout the whole lanthanide series produced till now only the unusual fluoride selenite $Gd_3(SeO_3)_4F$ (8). Now we have obtained another example of this type of structure and, furthermore, we were able to determine the structure of the new anhydrous selenite, $Er_2(SeO_3)_3$.

EXPERIMENTAL

Powder samples of the selenates $M_2(SeO_4)_3$ (M= Dy, Er) were obtained by dissolving M_2O_3 in a 20% solution of selenic acid. The solution was evaporated and the residue was dried under vacuum at 300°C. Two hundred milligrams of this powder was mixed with LiF in a molar ratio of 1:2 and sealed in a gold ampoule which was finally coated with a quartz glass ampoule. The ampoule was fired at 870°C in a resistance furnace for 10 h and then allowed to cool down slowly (2°C/h to 500°C, 5°C/h to 30°C). The gold ampoules were expanded remarkably after the reaction, hinting at the evolution of oxygen. The products contained single crystals showing the respective color of the rare earth ion (Dy: colorless, Er: pink) and a small amount of non–crystalline material. Single crystals of each product were prepared in glass capillaries (d= 0.1 mm). The quality of the single crystals was checked by orientation measurements on an image plate diffractometer (STOE IPDS). For

[1] To whom correspondence should be addressed. Fax: +0221-470-5083. E-mail: mathias.wickleder@uni-koeln.de.

0022-4596/02 $35.00

TABLE 1
$Er_2(SeO_3)_3$ and $Dy_3(SeO_3)_4F$: Crystallographic Data and Their Determination

Empirical formula	$Er_2(SeO_3)_3$	$Dy_3(SeO_3)_4F$
Formular weight (g/mol)	715.40	1014.34
Unit-cell parameters	a= 698.2(1) pm	a= 1036.0(1) pm
	b= 800.6(1) pm	c= 686.47(7) pm
	c= 895.0(1) pm	
	α= 71.38(1)°	
	β= 70.13(1)°	
	γ= 65.87(1)°	
Molar volume (cm^3/mol)	127.4	192.1
Z	2	2
Crystal shape	Irregular	Rod
Crystal size (mm^3)	0.1 × 0.1 × 0.15	0.1 × 0.1 × 0.2
Crystal system	Triclinic	Hexagonal
Space group	$P\bar{1}$ (No. 2)	$P6_3mc$ (No. 186)
Measuring device	Stoe IPDS II	Stoe IPDS I
Radiation	Mo$K\alpha$ (graphite monochromator; λ = 71.07 pm)	
Temperature (K)	293	
2θ range	$5° < 2\theta < 56°$	$7° < 2\theta < 56°$
Index range	$-11 \le h \ge 11$	$-13 \le h \ge 13$
	$-12 \le k \ge 12$	$-13 \le k \ge 11$
	$-14 \le l \ge 14$	$-8 \le l \ge 7$
φ-range; φ-increment	$0° < \omega < 180°$; 2° (2 runs at φ = 0°, 90°)	$0° < \varphi < 160°$; 2°
Number of exposures	180	80
Irradiation/exposure (min)	6	4.5
Detector distance (mm)	60	
Absorption correction	Numerical, after crystal shape optimization (12,11)	
Absorption coefficient (mm^{-1})	32.88	28.86
T_{min}/T_{max}	0.0184/0.0947	0.0400/0.0941
Measured reflections	6538	4431
Unique reflections,	1604	563
Observed with $I > 2\sigma(I)$	1403	545
R_{int}	0.0696	0.0703
Structure determination	SHELXS-86 and SHELXL-93 (9, 10)	
Scattering factors	Intern. Tables., Vol. C (13)	
Goodness-of-fit	1.099	1.435
R_1; $wR_2(I_0 > 2\sigma(I))$	0.0288; 0.0700	0.0299; 0.0746
R_1; wR_2 (all data)	0.0364; 0.0774	0.0305; 0.0748
Extinction coefficient	0.0033(4)	0.0084(8)
Flack-X parameter		0.04(7)
Depositiory no.	CSD 411749	CSD 411748

the best specimen, intensity data were collected using the same diffractometer. The structure solutions were successful in space group $P\bar{1}$ for $Er_2(SeO_3)_3$ and in the acentric space group $P6_3mc$ for the fluoride selenite $Dy_3(SeO_3)_4F$ with direct methods provided by the program SHELXS86 (9). The refinement was carried out using SHELXL93 (10). Finally, numerical absorption corrections were applied to the data with the help of the programs X-SHAPE (11) and X-RED (12). Since the crystals showed no well-defined faces, a dodecahedron was used as starting polyhedron for the crystal shape optimization with X-SHAPE. The crystallographic data obtained are summarized in Tables 1–5. The structural features of $Dy_3(SeO_3)_4F$ clearly prove the acentricity of the compound (see structure description). Additionally, the data have been deposited with the Fachinformationszentrum, Karlsruhe, D-76344 Eggenstein-Leopoldshafen (crysdata@FIZ-Karlsruhe.de) and are available on quoting the deposition numbers given

TABLE 2
Atomic Coordinates and Equivalent Displacement Parameters for $Er_2(SeO_3)_3$

Atom	x/a	y/a	z/a	$U_{eq} \times 10^{-1}$ pm^{-2}
Er1	0.25922(5)	0.26415(5)	0.20101(5)	9.4(1)
Er2	0.66671(6)	0.27064(5)	0.41072(5)	9.6(1)
Se1	0.1129(1)	0.2429(1)	0.5861(1)	10.2(2)
Se2	0.8541(1)	0.2474(1)	0.0345(1)	9.8(2)
Se3	0.5718(3)	0.2244(2)	0.8015(2)	22.5(3)
O11	0.3409(9)	0.2540(10)	0.4377(9)	15(1)
O12	0.9654(10)	0.2968(11)	0.4462(9)	19(1)
O13	0.1574(12)	0.0143(11)	0.6554(9)	22(2)
O21	0.9338(9)	0.3048(10)	0.1674(8)	14(1)
O22	0.5946(9)	0.2870(10)	0.1481(9)	17(1)
O23	0.8330(10)	0.4303(9)	0.8822(9)	15(1)
O31	0.4838(10)	0.4053(9)	0.6500(9)	17(1)
O32	0.6407(11)	0.0571(9)	0.6942(8)	12(1)
O33	0.3482(11)	0.2088(11)	0.9463(9)	18(2)

Note. $U_{eq} = \frac{1}{3}[U_{11}(aa^*)^2 + U_{22}(bb^*)^2 + U_{33}(cc^*)^2 + 2U_{12}aba^*b^* \cos\gamma + 2U_{13}abc^*c^* \cos\beta + 2U_{23}bcb^*c^* \cos\alpha]$. All atoms occupy the site 2*i*.

TABLE 3
Selected Distances (pm) and Angles (deg) for $Er_2(SeO_3)_3$

Er1–O11(b)	234.4(7)	Er2–O11(b)	225.9(5)
O12(b)	244.1(7)	O12(f)	231.2(7)
O21(c)	227.1(5)	O13(g)	226.7(8)
O22(a)	229.9(5)	O21(a)	236.0(6)
O23(d)	219.7(7)	O22(a)	251.9(7)
O32(c)	232.8(7)	O31(d)	232.1(7)
O33(a)	228.8(7)	O31(f)	242.3(8)
		O3(h)	256.2(7)
Se1–O11(a)	170.6(6)	O11–Se1–O12	92.4(3)
O12(a)	172.7(7)	O11–Se1–O13	103.9(4)
O13(a)	166.5(8)	O12–Se1–O13	101.9(4)
Se2–O21(a)	171.5(6)	O21–Se2–O22	93.8(3)
O22(a)	170.3(6)	O21–Se2–O23	104.1(3)
O23(a)	164.6(7)	O22–Se2–O23	103.0(3)
Se3–O31(a)	170.5(7)	O31–Se3–O32	93.6(3)
O32(a)	171.8(7)	O31–Se3–O33	105.6(3)
O33(a)	167.5(7)	O32–Se3–O33	105.9(3)

Note. (a) x, y, z; (b) $x-1, y, z+1$; (c) $x-1, y, z$; (d) $-x+1, -y+1, -z$; (e) $-x+1, -y, -z$; (f) $x, y, z+1$; (g) $-x+2, -y, -z$; (h) $x+1, y, z$.

TABLE 4
Atomic Coordinates and Equivalent Displacement Parameters for $Dy_3(SeO_3)_4F$

Atom	Site	x/a	y/a	z/a	U_{eq} 10^{-1} pm^{-2}
Dy1	6*c*	0.07482(6)	0.53741(3)	0.3181(1)	15.1(2)
Se1	2*b*	$\frac{1}{3}$	$\frac{2}{3}$	0.7531(4)	11.2(5)
Se2	6*c*	0.15448(8)	0.3090(2)	0.0842(2)	19.0(3)
O1	6*c*	0.4191(6)	0.5809(6)	0.642(2)	23(2)
O2	6*c*	0.1814(6)	0.363(1)	0.322(2)	28(2)
O3	12*d*	0.3347(8)	0.4168(8)	0.013(1)	21(2)
F1	2*b*	$\frac{1}{3}$	$\frac{2}{3}$	0.271(2)	18(4)

Note. $U_{eq} = \frac{1}{3}[U_{11} + U_{22} + U_{33}]$.

TABLE 5
Selected Distances (pm) and Angles (deg) for $Dy_3(SeO_3)_4F$

Dy1–F1(a)		234.1(2)	Dy1–Dy1(h)		401.8(1)
–O1(b)		235.7(12)			(within the triangle)
–O1(c)		244.1(11)			
–O2(a,d)	(2 ×)	255.5(8)	Dy1–Dy1(f)		368.6(1)
–O3(e,f)	(2 ×)	233.1(7)			(between the triangles)
–O3(a,g)	(2 ×)	245.8(8)			
Sel–O1(a,h,d)	(3 ×)	171.8(11)	O1–Se1–O1	(3 ×)	101.9(5)
Se2–O2(a)		170.1(15)	O2–Se2–O3	(2 ×)	96.5(4)
–O3(a,i)	(2 ×)	169.9(7)	O3–Se2–O3		100.8(5)

Note. (a) x, y, z; (b) $-y+1, x-y, z+1$; (c) $y+1, -x+y+1, z+\frac{1}{2}$; (d) $-x+y+1, -x+1, z$; (e) $-x+2, -x+y+1, z+\frac{1}{2}$; (f) $-x+2, -y+1, z+\frac{1}{2}$; (g) $x, x-y, z$; (h) $-y+1, x-y, z$; (i) $-x+y+1, y, z$.

TABLE 6
IR Data (cm^{-1}) for $Er_2(SeO_3)_3$ and $Dy_3(SeO_3)_4F$

Assignment for C_{3v} symmetry			
$Er_2(SeO_3)_3$			$Dy_3(SeO_3)_4F$
	372	$\nu_4(E)\delta_{as}$	
430 w			457 s
441 m	425	$\nu_2(A_1), \delta_s$	495 w
476 s			
503 w			
709 vs			718 s
763 m	740	$\nu_3(E), \nu_{as}$	749 s
796 s			802 s
837 s			827 s
854 w	810	$\nu_1(A_1), \nu_s$	860 m
855 w			877 m
894 w			

in Table 1. IR spectra were measured in the range of 4000–400 cm^{-1} with the help of the spectrometer IFS66v/s (BRUKER). For that purpose, KBr pellets containing small amounts of the samples were prepared. The observed frequencies are given in Table 6.

RESULTS AND DISCUSSION

Crystal Structures

In contrast to the powder diffraction investigations which suggested a monoclinic unit cell for $Er_2(SeO_3)_3$ (6), the present single–crystal investigation shows that the

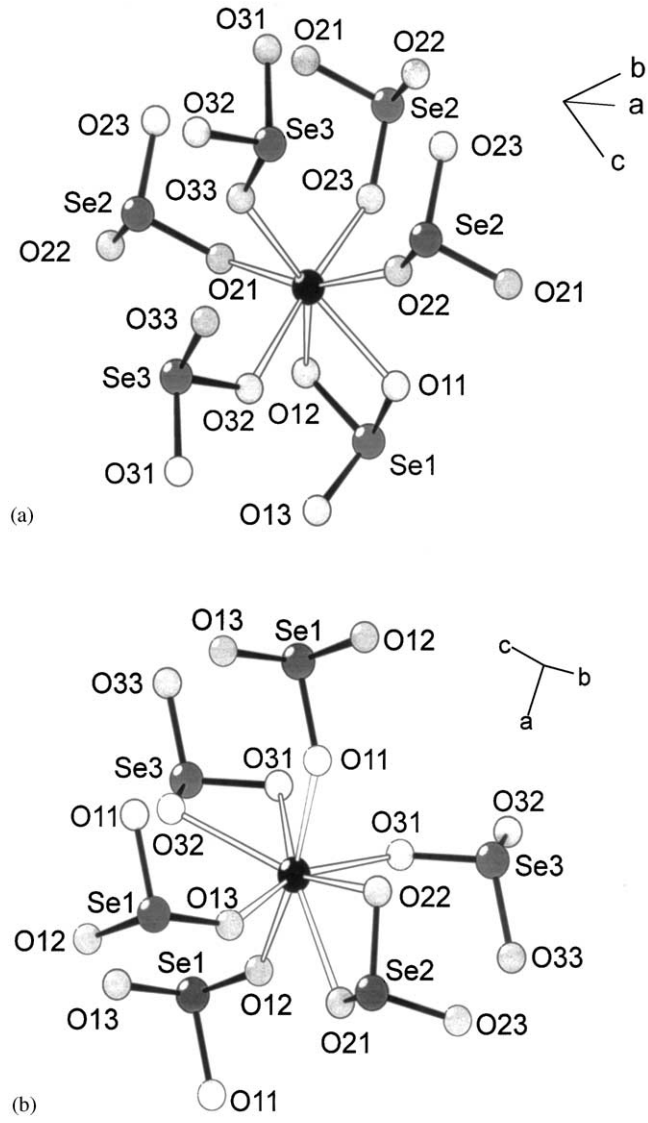

FIG. 1. Coordination of $Er(1)^{3+}$ (a) and $Er(2)^{3+}$ (b) in the crystal structure of $Er_2(SeO_3)_3$. Both ions are surrounded by six SeO_3^{2-} groups. The CNs are 7 and 8, respectively, because part of the selenite groups act as chelating ligands.

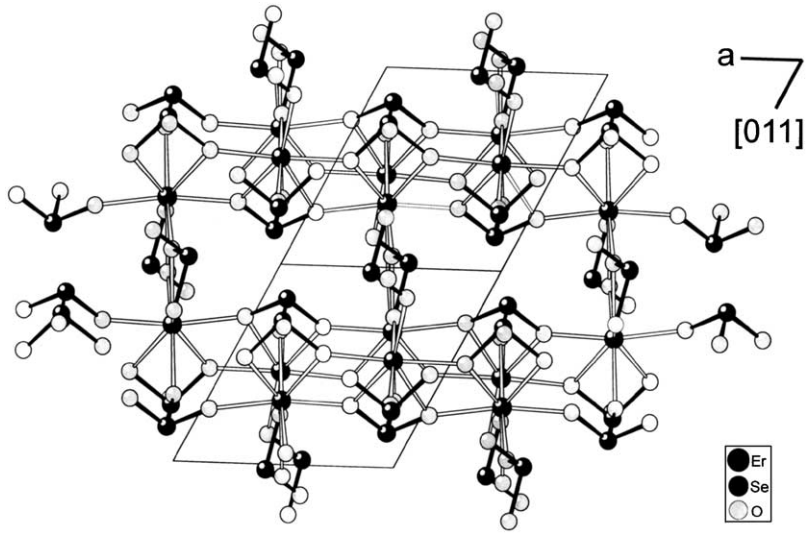

FIG. 2. Crystal structure of $Er_2(SeO_3)_3$ viewed along [01$\bar{1}$]. The linkage of the Er^{3+} polyhedra and the selenite ions lead to rectangular channels providing enough space to incorporate the lone pairs of the selenium atoms.

structure is triclinic and contains two crystallographically independent Er^{3+} ions and three crystallographically independent SeO_3^{2-} groups. The coordination spheres of $Er(1)^{3+}$ and $Er(2)^{3+}$ are shown in Fig. 1. $Er(1)^{3+}$ is coordinated by three $Se(2)O_3^{2-}$ and two $Se(3)O_3^{2-}$ groups and one $Se(1)O_3^{2-}$ ion (Fig. 1a). Since the latter acts as a chelating ligand, a coordination number of 7 results for $Er(1)^{3+}$. The coordination polyhedron can be seen as a pentagonal bipyramide with distances Er^{3+}–O^{2-} covering a range from 220 to 244 pm (Table 3). $Er(2)^{3+}$ is surrounded by oxygen atoms with distances from 226 to 256 pm. The oxygen atoms belong to three $Se(1)O_3^{2-}$, two $Se(3)O_3^{2-}$ and one $Se(2)O_3^{2-}$ groups, respectively. As two selenite ions ($1 \times Se(2)O_3^{2-}$, $1 \times Se(3)O_3^{2-}$) are attached in a chelating way, the coordination number of $Er(2)^{3+}$ is 8 (Fig. 1b). Each of the three crystallographically different selenite groups is attached to four Er^{3+} ions in such a way that all oxygen atoms of a selenite ion are monodentate

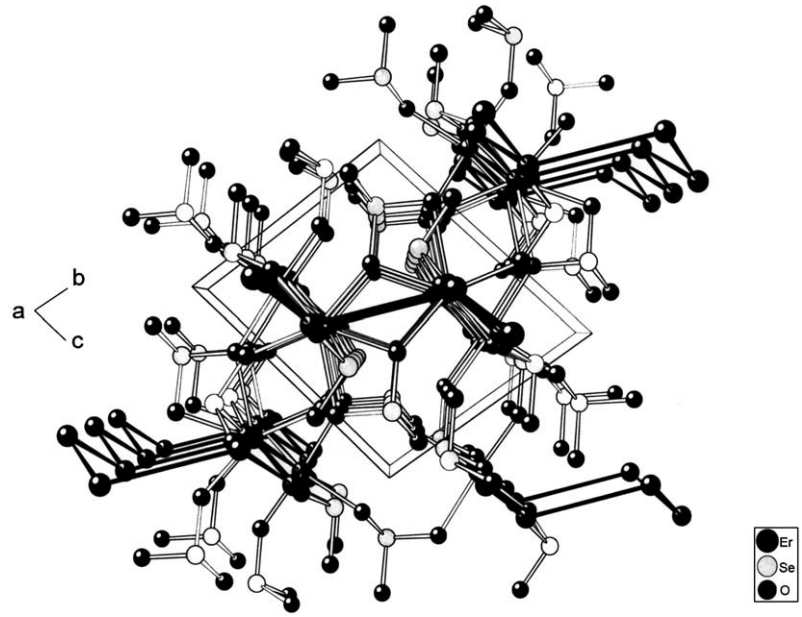

FIG. 3. Arrangement of the Er^{3+} ions in the crystal structure of $Er_2(SeO_3)_3$. Chains of edge-connected chairs are formed which extend in the [100] direction.

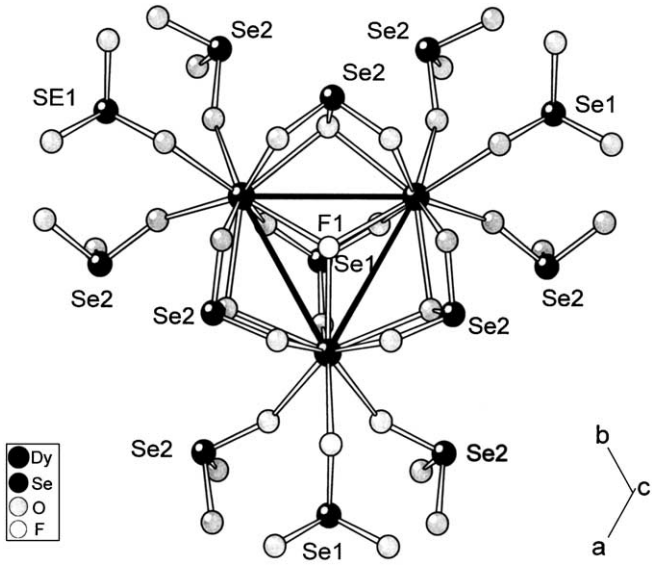

FIG. 4. $[Dy_3F(Se(1)O_3)_4(Se(2)O_3)_9]^{18-}$ unit in the crystals structure of $Dy_3(SeO_3)_4F$. The formation of the triangles is brought about by the selenite group $Se(1)O_3^{2-}$ which acts as a μ_3–ligand as well as by a $\mu_3 - F^-$ ion capping the triangle on the opposite side. The distances of the Dy^{3+} ions within the rings are 402 pm so that no bonding interaction can be supposed. Each edge of the ring is bridged by one oxygen atom of $Se(2)O_3^{2-}$ ion.

and two of them are additionally chelating. Note, that the exclusively monodentate oxygen atoms (O13, O23, and O33, respectively) show significantly shorter distances to the selenium atoms (Table 3). The three-dimensional structure of $Er_2(SeO_3)_3$ is shown in Fig. 2 in a projection along the $[0l\bar{1}]$ direction. The selenite ions $Se(1)O_3^{2-}$ and $Se(2)O_3^{2-}$ link the Er^{3+} ions to zig-zag chains along [100]. The Er^{3+}–Er^{3+} distances in that direction are 390 and 393 pm, respectively. Further linkage of the zig-zag chains occurs via the $Se(3)O_3^{2-}$ groups leading to Er^{3+}–Er^{3+} distances of 397 pm. If one connects all Er^{3+} ions with a distance below 400 pm, another interesting feature of the crystal structure comes up: the Er^{3+} ions form chains of edge-connected chairs in the [100] direction which are separated in the [010] direction by 454 pm and in the [001] direction by 555 pm (Fig. 3). A further characteristic feature of the crystal structure is the stereochemical activity of the lone pairs of the selenium atoms. As Fig. 3 reveals, the linkage of the Er^{3+} polyhedra and the selenite ions leads to rectangular channels in the $[01\bar{1}]$ direction providing enough space to incorporate the lone pairs. A very similar influence of the lone pairs on the crystal structure has been observed for $La_2(SeO_3)_3$ and $LaFSeO_3$, respectively. Also in these compounds, channels are formed which incorporate the lone pairs of the selenium atoms. However, because of the different ionic radii of La^{3+} and Er^{3+}, the coordination numbers of the La^{3+} ions are as high as 10 and 11 in the lanthanum compounds leading to different crystal structures.

$Dy_3(SeO_3)_4F$ is isotypic with the respective gadolinium compound, $Gd_3(SeO_3)_4F$. The crystal structure $Dy_3(SeO_3)_4F$ contains Dy^{3+} ions in triangular formation caused by the selenite group $Se(1)O_3^{2-}$ which acts as a μ_3-ligand as well as by a $\mu_3 - F^-$ ion capping the triangle on the opposite side (Fig. 4). The distances of the Dy^{3+} ions within the rings are 402 pm so that no bonding interaction can be supposed. The F^- ion is shifted 30 pm out of the plane of the ring. Each edge of the ring is bridged by one oxygen atom of the crystallographically second selenite group, $Se(2)O_3^{2-}$ (Fig. 4). The remaining oxygen atoms of this selenite ion belong also to the coordination sphere of Dy^{3+} ions of the ring. The coordination sphere of the three Dy^{3+} ions is completed by three $Se(1)O_3^{2-}$ and six $Se(2)O_3^{2-}$ ligands, so that the building unit $[Dy_3F(Se(1)O_3)_4(Se(2)O_3)_9]^{18-}$ results. These fragments are stacked with the same orientation along [001], leading to the acentricity of the crystal structure (space group $P6_3mc$). The linkage of the fragments is performed by both selenite groups (Fig. 5). The capping $Se(1)1O_3^{2-}$ group connects one ring to three others so that each oxygen atom of the anion is bidentate bridging while $Se(2)O_3^{2-}$ links two other triangles in such a way that all oxygen atoms of the group are monodentate and two of them additionally chelating ligands. Thus, the connectivity can be written as $Dy_3F(Se(1)O_3)_{4/4}(Se(2)O_3)_{9/3}$ according to *Niggli's*

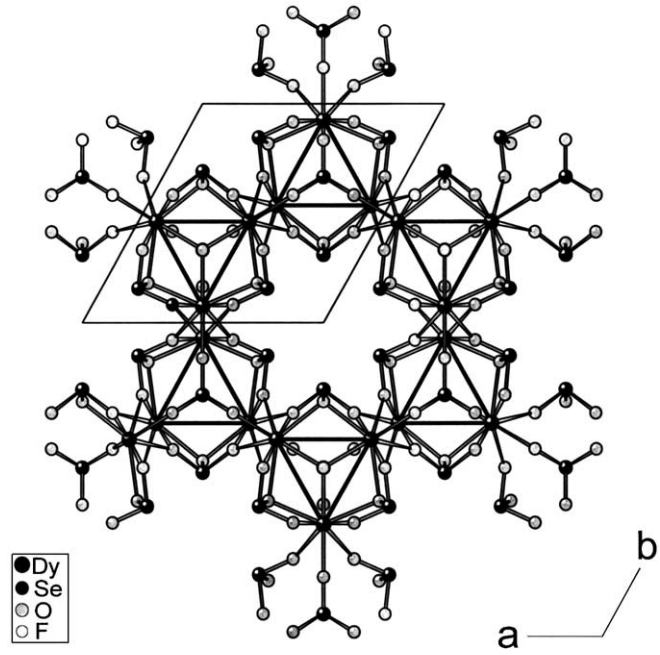

FIG. 5. Crystal structure of $Dy_3(SeO_3)_4F$ viewed along [001]. The hexagonal channels are 663 pm in diameter and incorporate the lone pairs of the $Se(2)O_3^{2-}$ groups.

formalism. Note, that the distances of two Dy^{3+} ions between two rings are with 368 pm remarkably shorter than those within the rings. The close proximity of the ions is due to their linkage by three oxygen atoms.

The influence of the lone pairs of the Ψ^1-tetrahedral anion is even more prominent than found for $Er_2(SeO_3)_3$. The lone pair of the $Se(1)O_3^{2-}$ ion is oriented along [001] in the direction to the fluoride ion so that a very long distance Se–F of 369 pm results. The lone pairs of the $Se(2)O_3^{2-}$ ions are incorporated in channels which run parallel to the [001] direction. The diameter of these channels are 663 pm with respect to the opposite selenium atoms.

IR Spectra

For a SeO_3^{2-} ion with ideal C_{3v} symmetry, four normal modes can be expected which belong to the symmetry species A_1 and E (14). In solution the stretching vibrations, ν_s and ν_{as}, are found at 810 and 740 cm^{-1} while the bending modes, δ_s and δ_{as}, are located at 425 and 372 cm^{-1} (15). The latter were not observable within the range of the MIR measurements performed (4000–400 cm^{-1}). For the remaining three modes, a splitting of the bands is observed in the spectra of $Er_2(SeO_3)_3$ and $Dy_3(SeO_3)_4F$ due to the lowering of the SeO_3^{2-} symmetry. In $Er_2(SeO_3)_3$, all of the selenite ions exihibit C_1 symmetry while in $Dy_3(SeO_3)_4F$ the μ_3-$Se(1)O_3^{2-}$ ligand has C_{3v} and the $Se(2)O_3^{2-}$ ion C_s symmetry. Furthermore, a factor group splitting may occur. The observed frequencies match very well the values known for various selenites (16) and in particular the data known for the rare earth selenites investigated so far (17). In Table 6, the observed bands for both compounds are given together with the assignment based on C_{3v} symmetry and the typical values for SeO_3^{2-} in solution.

ACKNOWLEDGMENTS

The authors are indebted to Prof. Dr. G. Meyer, to the *Deutsche Forschungsgemeinschaft (Graduiertenkolleg 549 "Azentrische Kristalle")*, and to the *Fonds der Chemischen Industrie, Frankfurt am Main*, for generous support. The technical assistance of Mrs. I. Müller is also gratefully acknowledged.

REFERENCES

1. M. S. Wickleder, *Z. Anorg. Allg. Chem.* **624,** 1347–1354 (1998); M. S. Wickleder, *Z. Anorg. Allg. Chem.* **626,** 1468–1472 (2000).
2. M. S. Wickleder, *Z. Anorg. Allg. Chem.* **625,** 93–96 (1999); M. S. Wickleder, *Z. Anorg. Allg. Chem.* **625,** 302–308 (1999); M. S. Wickleder, *Z. Anorg. Allg. Chem.* **625,** 725–728 (1999); M. S. Wickleder, *Z. Anorg. Allg. Chem.* **626,** 1723–1724 (2000).
3. M. A. Nabar and S. V. Paralkar, *Thermochim. Acta* **17,** 239–246 (1976); M. A. Nabar and S. V. Paralkar, *Thermochim. Acta* **15,** 390–392 (1976); B. Hájek, N. Novotna, and J. Hradilová, *J. Less-Common Met.* **66,** 121–136 (1979).
4. M. S. Wickleder, *Z. Anorg. Allg. Chem.* **626,** 547–551 (2000).
5. E. Giesbrecht, M. Perrier, and W. W. Wendlandt, *Anais Acad. Bras. Cienc.* **34,** 37–43 (1962); E. Giesbrecht and I. Giolito, *Anais Acad. Bras. Cienc.* **39,** 233–239 (1967); I. A. Maier, Yu. L. Suponitskii, and M. Kh. Karapet'yants, *Izv. Vyssh. Uchebn. Zaved. Khim. Khim. Tekhnol.* **14,** 3–7 (1971).
6. G. S. Savchenko, I. V. Tananaev, and A. N. Volodina, *Izv. Akad. Nauk SSSR Neorgan. Mater.* **4,** 1097–1107 (1968); *Inorg. Mater. [USSR]* **4** (1968), 965–972; E. Giesbrecht, G. Vicentini, and L. Barbieri, *Anais Acad. Bras. Cienc.* **40,** 453–459 (1968); M. de Pedro, R. Enjalbert, A. Castro, J.-C. Trombe, and J. Galy, *J. Solid State Chem.* **108,** 87–93 (1994); A. Castro, R. Enjalbert, M. de Pedro, and J.-C. Trombe, *J. Solid State Chem.* **108,** 418–423 (1994); M. de Pedro, J.-C. Trombe, and A. Castro, *J. Mater. Sci. Lett.* **14,** 994–997 (1995); M. de Pedro, I. Rasines, and A. Castro, *J. Mater. Sci. Lett.* **12,** 1637–1640 (1993).
7. H. Oppermann and M. Zhang-Preße, *Naturforscher,* **56b,** 917–926 (2001); H. Oppermann, M. Zhang-Preße, S. Weck, and S. Liebig, *Z. Anorg. Allg. Chem.* **628,** 81–90 (2002); M. Zhang-Preße, Dr. rer. nat. Thesis, Universität Dresden, 2001.
8. M. S. Wickleder and I. Göhausen, *Z. Anorg. Allg. Chem.* **626,** 1725–1727 (2000).
9. G. M. Sheldrick, "SHELXS86, Programme zur Röntgenstrukturanalyse." Göttingen, 1986.
10. G. M. Sheldrick, "SHELXL93, Program for the Refinement of Crystal Structures." Göttingen, 1993.
11. "X-SHAPE 1.01, Crystal Optimisation for Numerical Absorption Correction." Stoe & Cie, Darmstadt, 1996.
12. "X-RED 1.07, Data Reduction for STADI4 and IPDS." Stoe & Cie, Darmstadt, 1996.
13. Th. Hahn, Ed., "International Tables for Crystallography," Vol. C. D. Reidel Publishing Company, Dordrecht, Boston, 1983.
14. J. Weidlein, U. Müller, and K. Dehnicke, "Schwingungsspektroskopie." Thieme, Stuttgart, New York, 1988.
15. H. Siebert, "Anwendung der Schwingungsspektroskopie in der Anorganischen Chemie", p. 57. Springer, Berlin, Heidelberg, New York, 1966.
16. K. Sathianandan, L. D. McCory, and J. L. Margrave, *Spectrochim. Acta* **20,** 957–963 (1964).
17. V. P. Verma, *Thermochim. Acta* **327,** 63–102 (1999) and references therein.